NEOPLASIA
www.neoplasia.com

Volume 23 Number xxx Month 2021 pp. 348–359



**Original Research**

# High dose acetaminophen inhibits STAT3 and has free radical independent anti-cancer stem cell activity

Pavani Pingali[a,#]; Y. Jeffrey Wu[b,#]; Rio Boothello[a]; Chetna Sharon[a]; Howard Li[c,d]; Srinivas Sistla[f]; Nehru Viji Sankaranarayanan[f]; Umesh R. Desai[f,g]; Anh T. Le[h]; Robert C. Doebele[h]; Leslie L. Muldoon[b]; Bhaumik B. Patel[a,e,*]; Alexander Neuwelt[a,e,*]

[a] Section of Hematology and Oncology, Medicine Service, Hunter Holmes McGuire VA Medical Center, Richmond, VA
[b] Department of Neurology, OHSU, Portland, OR
[c] Department of Pulmonology, Hunter Holmes McGuire VA Medical Center, Richmond, VA
[d] Department of Pulmonology, Virginia Commonwealth University Hospital, Richmond, VA
[e] Division of Hematology, Oncology, and Palliative care, Department of Medicine, and Massey Cancer Center, Virginia Commonwealth University. Richmond, VA
[f] Institute for Structural Biology, Drug Discovery and Development, Virginia Commonwealth University, Richmond, VA
[g] Department of Medicinal Chemistry, School of Pharmacy, Virginia Commonwealth University, Richmond, VA
[h] Division of Medical Oncology, Department of Medicine, University of Colorado Anschutz Medical Campus, Aurora, CO

## Abstract

High-dose acetaminophen (AAP) with delayed rescue using n-acetylcysteine (NAC), the FDA-approved antidote to AAP overdose, has demonstrated promising antitumor efficacy in early phase clinical trials. However, the mechanism of action (MOA) of AAP's anticancer effects remains elusive. Using clinically relevant AAP concentrations, we evaluated cancer stem cell (CSC) phenotype in vitro and in vivo in lung cancer and melanoma cells with diverse driver mutations. Associated mechanisms were also studied. Our results demonstrated that AAP inhibited 3D spheroid formation, self-renewal, and expression of CSC markers when human cancer cells were grown in serum-free CSC media. Similarly, anti-CSC activity was demonstrated in vivo in xenograft models - tumor formation following in vitro treatment and ex-vivo spheroid formation following in vivo treatment. Intriguingly, NAC, used to mitigate AAP's liver toxicity, did not rescue cells from AAP's anti-CSC effects, and AAP failed to reduce glutathione levels in tumor xenograft in contrast to mice liver tissue suggesting nonglutathione-related MOA. In fact, AAP mediates its anti-CSC effect via inhibition of STAT3. AAP directly binds to STAT3 with an affinity in the low micromolar range and a high degree of specificity for STAT3 relative to STAT1. These findings have high immediate translational significance concerning advancing AAP with NAC rescue to selectively rescue hepatotoxicity while inhibiting CSCs. The novel mechanism of selective STAT3 inhibition has implications for developing rational anticancer combinations and better patient selection (predictive biomarkers) for clinical studies and developing novel selective STAT3 inhibitors using AAP's molecular scaffold.

*Neoplasia (2021) 23, 348–359*

**Keywords:** Acetaminophen, N-acetylcysteine, STAT3, Cancer stem cells

*Abbreviations:* AAP, acetaminophen; CSC, cancer stem cell; LDA, limiting dilution assay; NAC, n-acetylcysteine; NSCLC, nonsmall cell lung cancer; STAT3, signal transducer and activator of transcription 3.

* Corresponding authors.
E-mail addresses: Bhaumik.patel@va.gov (B.B. Patel), alexander.neuwelt@va.gov (A. Neuwelt).
# These authors contributed equally to this manuscript.

Received 24 November 2020; received in revised form 3 February 2021; accepted 5 February 2021



https://doi.org/10.1016/j.neo.2021.02.001

## Introduction

The use of high-dose acetaminophen (AAP) as an anticancer agent has been studied both preclinically and clinically [1–3]. In a phase I clinical trial involving a variety of cancer histologies, single agent high-dose AAP induced an objective response in 3 out of 14 assessable patients (21%), defined as regression of all sites of measurable disease by at least 50%. AAP was followed by delayed rescue with N-acetylcysteine (NAC), the established antidote for AAP overdose-induced liver toxicity, and no dose limiting toxicity was observed despite treating patients with up to 20 g/m$^2$ AAP [2]. Subsequently, a 3-year-old patient with hepatoblastoma that was cisplatin-refractory and had failed all standard therapies was treated with AAP 30 g/m$^2$ plus cisplatin with delayed NAC rescue. The patient had a near complete response and was alive and disease free 7 years later at the time of his case report [4].

Of note, the AAP doses used in clinical trials could not be used without NAC rescue. Hence, a concern may arise that NAC rescue would decrease the antitumor effects of AAP. Within the liver, AAP overdose leads to a buildup of a toxic free radical metabolite N-acetyl-p-benzoquinone imine (NAPQI). NAPQI gets detoxified by the antioxidant glutathione, leading to glutathione depletion and reactive oxygen species mediated hepatocellular injury [5]. NAC is a glutathione precursor and is thought to reverse AAP liver toxicity by replenishing glutathione stores. In contrast, our studies of tumor-bearing rats demonstrated that AAP induces glutathione depletion within the liver but not in the tumor [3]. The differential effects of AAP in the liver and the tumor is likely attributable to the relatively selective expression of CYP2E1, the enzyme responsible for metabolizing AAP into NAPQI, in the liver [6]. However, if the antitumor activity of high-dose AAP is not mediated by glutathione depletion, then an alternate mechanism must exist that has yet to be determined.

Within the heterogeneous tumor microenvironment, a population of pluripotent cancer stem cells (CSCs) reside [7]. CSCs are implicated in many aggressive cancer behaviors, including metastasis [8,9] and resistance to chemotherapy leading to cancer regrowth even in tumors with an initial chemotherapeutic response [10]. Hence, molecules that inhibit CSC phenotype may significantly improve cancer-related outcomes. There are no agents with known anti-CSC effects approved by FDA for solid tumors, including nonsmall cell lung cancer. As AAP (with NAC rescue) demonstrated single-agent activity in patients with relapsed/refectory cancer and prevented regrowth of tumor in rats following chemotherapy [3], it is intriguing to hypothesize that AAP may have anti-CSC properties.

Signal transducer and activator of transcription 3 (STAT3) signaling is required for the growth, proliferation and maintenance of CSCs [11,12]. STAT3 overexpression contributes to poor prognosis among different types of cancer [13], and appears to play a critical role in nonsmall cell lung cancer (NSCLC) [14] and skin cancer [15] pathogenesis and progression. Interleukin-6 (IL-6) is a multi-functional cytokine within the tumor microenvironment and a key stimulus of STAT3 signaling. Elevated levels of IL-6 are associated with cancer cell proliferation, angiogenesis, invasiveness and metastasis through the STAT3 and MAPK signaling pathways [16].

In the current study, we demonstrate that high-dose AAP has anti-CSC activity via inhibition of STAT3. This effect was preserved with concurrent administration of NAC.

## Materials and methods

### *Cell line culture and reagents*

Human A2058 melanoma, H460 NSCLC, A549 NSCLC, and H1975 NSCLC cells were obtained from the American Type Culture Collection (Manassas VA, USA). CUTO29 NSCLC cells were obtained from the lab of Dr. Robert Doebele. CUTO29 cells were derived from a patient progressing on brigatinib from neck lymph node and next-generation sequencing identified an *EML4-ALK* (E6:A19) fusion. All cells were cultured with proper medium supplemented with 10% fetal bovine serum (HyClone, Logan, UT) and 1% penicillin/streptomycin. Cells were confirmed mycoplasma-free, used at low passage, harvested immediately prior to implantation and used only if viability exceeded 90%. For in vitro assays, powdered AAP (Sigma, St. Louis, MO) was dissolved in DMSO and sterile filtered through a 0.2 μm membrane. For rat animal studies, liquid AAP (PediaCare infant formulation) was obtained from the Oregon Health and Sciences University (OHSU) pharmacy. Sterile cisplatin, NAC and sodium thiosulfate (STS) were obtained from the OHSU pharmacy. STAT3 inhibitor AG490, recombinant human IL-6 and interferon $\gamma$ were purchased from ThermoFisher Scientific Inc. and L-buthionine sulfoximine (BSO; 50 mg/mL) was from Ben Venue Laboratory (Bedford, OH).

### *shRNA STAT3 KD*

STAT3 H460 cells were grown overnight to ∼40% confluence and transiently transfected with scrambled or STAT3 ShRNAs (Cat # RHS4531-EG6774, Dharmacon, Lafayette, CO). Transfection was performed using DharmaFECTkb transfection reagent (Cat # T-2006-01, Dharmacon, Lafayette, CO) according to manufacturer's protocol.

### *In vitro tumor sphere formation assay*

Single-cell suspensions of A2058, A549, CUTO 29 and H460 cells (lower than passage 10) or tumor cells isolated from subcutaneous tumors were plated in ultra-low attachment plates (Corning, Acton, MA) in serum-free DMEM/F12 medium (Invitrogen, Carlsbad, CA) supplemented with 20 ng/mL epidermal growth factor (Sigma, St Louis, MO), 10 ng/mL basic fibroblast growth factor (Sigma), 5 $\mu$g/mL insulin (Sigma), B27 supplement (1:50 dilution, ThermoFisher Scientific) and 0.4% bovine serum albumin (Sigma). Approximately 3-d post plating, the spheroids measuring between 50 and 150 microns were counted in each 96-well by examining the whole well. Half-maximal inhibitory concentration ($IC_{50}$) values for spheroid formation in CSC media were calculated using SigmaPlots.

### *Extreme limiting dilution analysis*

Single cell suspension was plated at a concentration of 128, 64, 32, 16, 8, 4, 2, and 1 cell per 100 μL stem cell media in a 96 well ultra-low attachment plate and incubated for 5 d. After 5 d, the number of wells showing tumor spheres 50 to 150 $\mu$m was counted. The frequency of spheroid forming cells was determined using ELDA webtool [17].

### *In vitro WST-1 cell viability assay and $IC_{50}$ analysis*

WST assay was performed using our previously published methods [1]. $IC_{50}$ values were calculated by fitting a four-parameter dose response curve to normalized data using GraphPad Prism software.

### *Western blot analysis*

Western blotting was performed using our previously published methodologies [1]. Antibodies for immunoassay are listed in Supplementary Methods.

### *Immunofluorescent microscopy*

Cancer cells were grown in a Lab-Tek II chamber slide system (Nalge Nunc International, Rochester, NY). Cells were fixed in 4% paraformaldehyde for 15 min, permeabilized with 0.3% Triton X-100 and

blocked in PBS containing 2% bovine serum albumin for 30 min. The samples were then incubated with primary antibodies at the manufacturer's recommended dilution in PBS- bovine serum albumin at 4°C overnight. After incubation with the primary antibody, cells were washed and counterstained with the respective secondary antibody conjugated with Alexa Fluor 484 or 594 (Molecular Probes, Eugene, OR) and Hoechst nuclei stain. Images were captured on the EVOS FL fluorescent microscope under the identical exposure time (ThermoFisher Scientific). Six randomly selected fields were reviewed and data were analyzed using PRISM software. Nuclear STAT3 was determined as colocalization of pSTAT3 with DAPI nuclei stain.

### *Real-time PCR*

Real-time PCR was performed using previously published methodologies [18]. Primers used are contained in Supplementary Methods. The quantitative differences in mRNA expression of genes were calculated according to the comparative threshold (Ct) cycle method using GAPDH transcripts as endogenous controls.

### *Cellular thermal shift assay*

H460 NSCLC cells were grown in CSC media and treated with indicated drug for 6 h. Cells were then heated to indicated temperature for 10 minutes followed by lysis with RIPA buffer and semi-quantitation of protein using Western blotting [19].

### *Microscale thermopheresis (MST)*

MST experiments were performed on a Monolith NT system in label-free mode (NanoTemper Technologies GmbH, Munich, Germany). Samples were prepared in the MST buffer (10 mM Tris HCl pH7.4; 100 mM NaCl; 10 mM MgCl2; 0.05% Tween-20) and loaded into premium-treated capillaries. Sufficient concentrations (~ 0.05–1.5 μM) of STAT3 and (~0.005–20 μM) of AAP were used to study changes in thermophoresis as a function of the ligand. Experiments were performed 3 times under independent conditions (biological replicates) to enhance rigor and ensure accuracy, while also scanning each capillary multiple times (technical replicates). Kds for protein – ligand complexes were calculated using analysis software from NanoTemper [20].

### *Glutathione assay*

Total glutathione levels were assessed using Glutathione Colorimetric Detection kit (Invitrogen, Cat# EIAGSHC). 10 mg of liver/tumor tissue was homogenized in ice cold 5% SSA (5-Sulfo-Salicyclic acid dehydrate), incubated for 10 min at 4°C. Samples were centrifuged at 14,000 rpm for 10 min and supernatants were collected for total Glutathione analysis.

### *Flow cytometry*

Cells were collected with trypsinization and stained with indicated antibody. For intracellular stains, cells were fixed (BD catalogue # 558049), and permeabilized (BD catalogue # 558050) prior to analysis. Alexa Fluor 647 Mouse Anti-Stat3 (pY705) (Cat# 557815, BD) and Alexa Fluor® 647 Mouse IgG2a, Isotype Control (Cat# 558053, BD) antibodies were used and flow cytometry was performed on BD canto II. The data were analyzed using FlowJO (Tree Star Inc.) software. For surface stains, cells were incubated with human CD133-APC (Cat# FAB11331A-100, R&D systems) conjugated antibody for 30 min at 4 °C and washed once with PBS buffer prior to analysis. Cell sorting was performed using FACSAria II High-Speed Cell Sorter (BD Biosciences, San Jose, CA) and data were analyzed with FCS Express 4 Flow Cytometry software (De-Novo Software, Los Angeles, CA).

### *Animal studies*

The in vivo experiments and procedures described here were carried out in accordance with the Institutional Animal Care and Use Committee and under the supervision of the Department of Comparative Medicine at OHSU and the Hunter Holmes McGuire animal research facility.

For the in vivo limiting dilution assay and glutathione assay, 10 wk old CrTac:NCr-Foxn1nu NCr Nude mice obtained from Taconic laboratories were injected subcutaneously with increasing amounts of H460 NSCLC cells and tumor formation was noted (yes/no). Data were analyzed using ELDA software.

For rat experiments, female (200–250 g) athymic (*rnu/rnu*) rats from the OHSU breeding colony were supplied with food and water ad libitum and housed in a room with a 12-h light:dark cycle maintained at 22 ± 2°C.

#### *Therapeutic effect of AAP treatment*

Cancer cells ($2.5 \times 10^7$) were suspended in saline and subcutaneously injected into the flanks of athymic rats, using a 27-gauge needle. Rats (n = 3 per group) were untreated (control) or given AAP (600 mg/kg; PO) with or without NAC (1000 mg/kg IV) right after AAP at day 10 and tumors were harvested at day 14 after tumor implantation.

#### *Impact of AAP pretreatment*

A2058 or H460 cells were untreated (control) or pretreated with AAP (10 mM) or AAP+NAC (1 mg/mL) for 2 h in vitro prior to inoculation of $2.5 \times 10^7$ cells subcutaneously into the right and left flank of the athymic rat (both flanks were used, and rats may have been inoculated with tumor cells undergoing either the same or different pretreatments in either flank). n = 6 per treatment group, except n = 5 for AAP+NAC with A2058 cells. Tumors were measured twice per week using calipers and their volumes were calculated using the following standard formula: ½ (length × width$^2$). Tumors were harvested at 17 d after implantation.

*Ex vivo analysis of tumor specimens.* After treatment, tumor samples were resected from animals upon sacrifice. Tumors were digested in collagenase at 37°C for 30 min and filtered through 60 μm strainer to obtain single cell suspension for in vitro tumor sphere formation assay. For western blot analysis, tumors were dissolved and homogenized in RIPA buffer with protease and phosphatase inhibitors [21].

*Proteome profiler phosphokinase array.* Phosphokinase array analysis was performed using Proteome Profiler Human Phospho-Kinase Array Kit (Catalog # ARY003B; R&D Systems Inc., Minneapolis, MN). Cells were treated with AAP (10 mM) or vehicle for 2 h, and then media was changed and IL6 (20 ng/mL) was added. Whole cell lysate was obtained after treatment and transferred to membrane following manufacturer's protocol. The signals were quantified using UN-SCAN-IT gel software 6.1 (Silk Scientific., Orem UT).

*Fluorescence spectra titrations.* Fluorescence spectra were recorded with a Horiba QM400 spectrometer (HORIBA Scientific Piscataway, New Jersey, USA) with a 280 nm excitation wavelength. The spectral bandwidths were 1.0 mm and 1.0 mm for excitation and emission, respectively. The fluorescence spectra of STAT3 and STAT1 (22 nM) were recorded in the wavelength range of 300 to 400 nm. AAP, C188-9, or ibuprofen was titrated into protein solution with increasing concentrations and spectra were recorded. The AAP, C188-9, and ibuprofen were all prepared fresh in DMSO such that the final reaction mixture contained less than 5% v/v organic solvent. The slit widths,

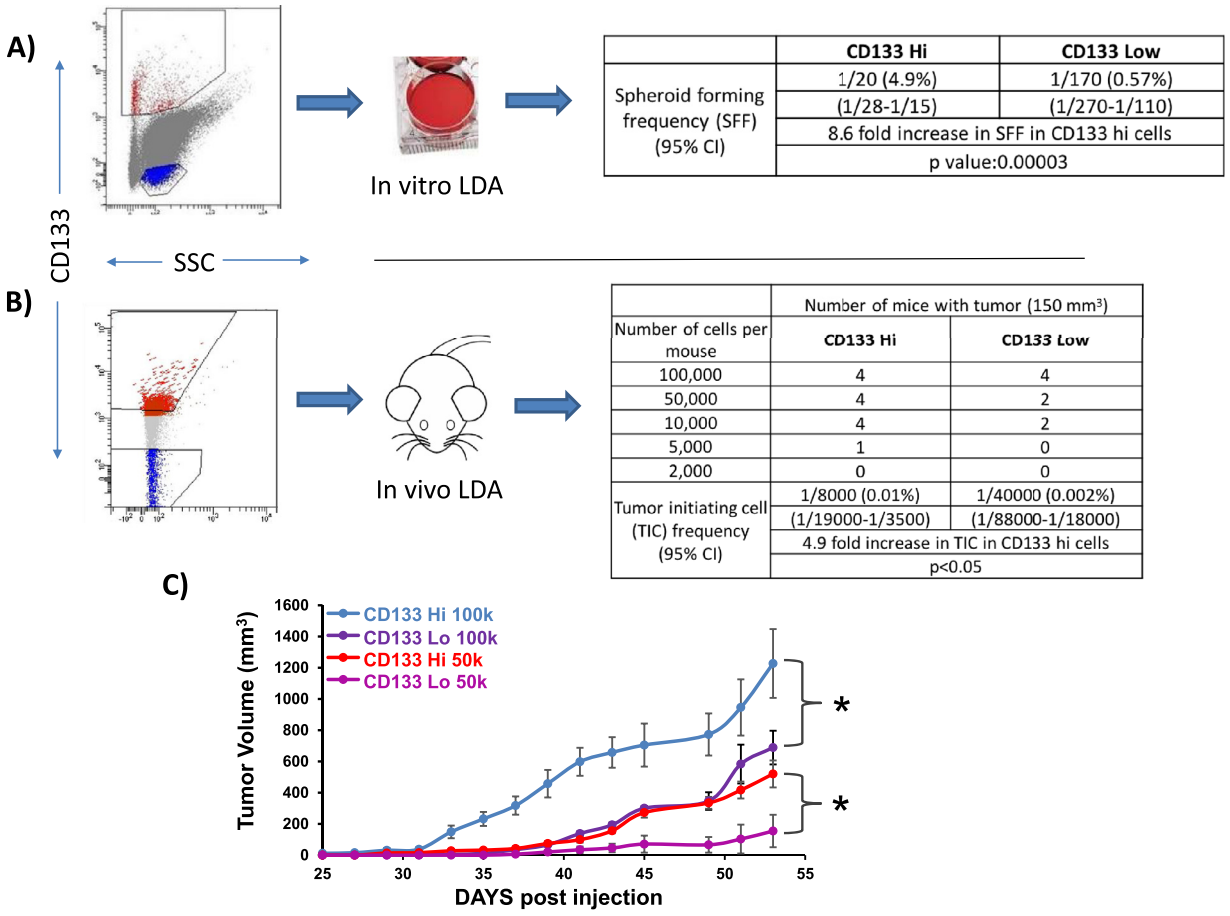


| | CD133 Hi | CD133 Low |
|---|---|---|
| Spheroid forming frequency (SFF) (95% CI) | 1/20 (4.9%) | 1/170 (0.57%) |
| | (1/28-1/15) | (1/270-1/110) |
| | 8.6 fold increase in SFF in CD133 hi cells | |
| | p value:0.00003 | |

| | Number of mice with tumor (150 mm³) | |
|---|---|---|
| Number of cells per mouse | CD133 Hi | CD133 Low |
| 100,000 | 4 | 4 |
| 50,000 | 4 | 2 |
| 10,000 | 4 | 2 |
| 5,000 | 1 | 0 |
| 2,000 | 0 | 0 |
| Tumor initiating cell (TIC) frequency (95% CI) | 1/8000 (0.01%) | 1/40000 (0.002%) |
| | (1/19000-1/3500) | (1/88000-1/18000) |
| | 4.9 fold increase in TIC in CD133 hi cells | |
| | p<0.05 | |

**Fig. 1.** CD133 is a cancer stem cell marker in nonsmall cell lung cancer cells. (**A**) H460 NSCLC cells were grown as spheroids in stem cell media and flow sorted for very high (red) or very low (blue) CD-133 expression with the indicated gating strategy. The CD133 positive and CD133 negative cells were plated at limiting dilutions (0→128 cells /well) and assessed for spheroid formation (yes/no). (**B**) The CD133 positive and CD133 negative cells were implanted into mice in limiting dilutions and assessed for tumor formation (yes/no). (**C**) Tumor growth curves of mice injected with indicated number of flow-sorted cells. * indicates $P < 0.05$.

excitation voltage, and scan speed were kept constant within each data set. All samples were measured in a stoppered quartz cuvette (path length 1 cm). Measurements were performed at 25°C. Titrations were performed manually using a micropipette. For each titration, the fluorescence emission spectrum of targets in the reaction solution was collected in 10 mM Tris HCl buffer, pH7.4, containing 100 mM NaCl, 10 mM $MgCl_2$, and 0.05% Tween-20. At least 3 independent experiments were performed to calculate standard errors. The emission spectra of protein are corrected for buffer and dilution effects. The observed change in fluorescence ($\Delta F$) relative to initial fluorescence ($F_0$) was fitted using a standard single-site binding model with a nonspecific component to obtain the apparent dissociation constant ($K_{D,app}$) and the maximal change in fluorescence ($\Delta F_{max}$) at saturation, as described earlier [22,23].

### *Statistical analysis*

All data are presented as mean ± S.D. The Student t test was used for the comparison of measurable variants between 2 groups. Two-way analysis of variance (ANOVA) followed by the Tukey test was used to evaluate differences among more than 3 groups. Two-way ANOVA with Bonferroni post-test was used for statistical comparisons between groups in tumor growth. $P < 0.05$ was considered statistically significant (GraphPad Prism 6.0; Graph Pad Software).

## Results

### *Validation of CD133 as a CSC marker in nonsmall cell lung cancer cells*

CD133 is a widely recognized CSC marker [24]. Cells grown in 3D spheroid cultures are significantly enriched in CSCs [25]. Indeed, H460 NSCLC cells grown as spheroids had significantly increased expression of CD133 relative to cells grown in standard monolayer conditions (Supplemental Figure 1).

In order to validate the use of CD133 as a CSC marker in NSCLC, an in vitro limiting dilution assay (LDA) was performed. H460 NSCLC cells were grown in CSC medium and flow sorted for CD133 high and low cells (Fig. 1). Sorted cells (highest 1% and lowest 3% of cells for CD133 expression) were plated into 96-well plates at limiting dilutions (0→128 cells /well) and assessed for spheroid formation (>50 $\mu$m) after a 4-day growth period. The results were analyzed according to the LDA protocol [17]. A 9-fold increase in the spheroid forming frequency (SFF) in the CD133 high versus low cells was observed, supporting the use of CD133 as a CSC marker in NSCLC (Fig. 1A). CD133 high cells had a 2.9-fold increase in SFF relative to CD133 intermediate cells, suggesting that the mixed population has an intermediate phenotype (Supplemental Figure 2). An in vitro LDA was also performed using A549 NSCLC cells (KRAS mutant, established cell line)

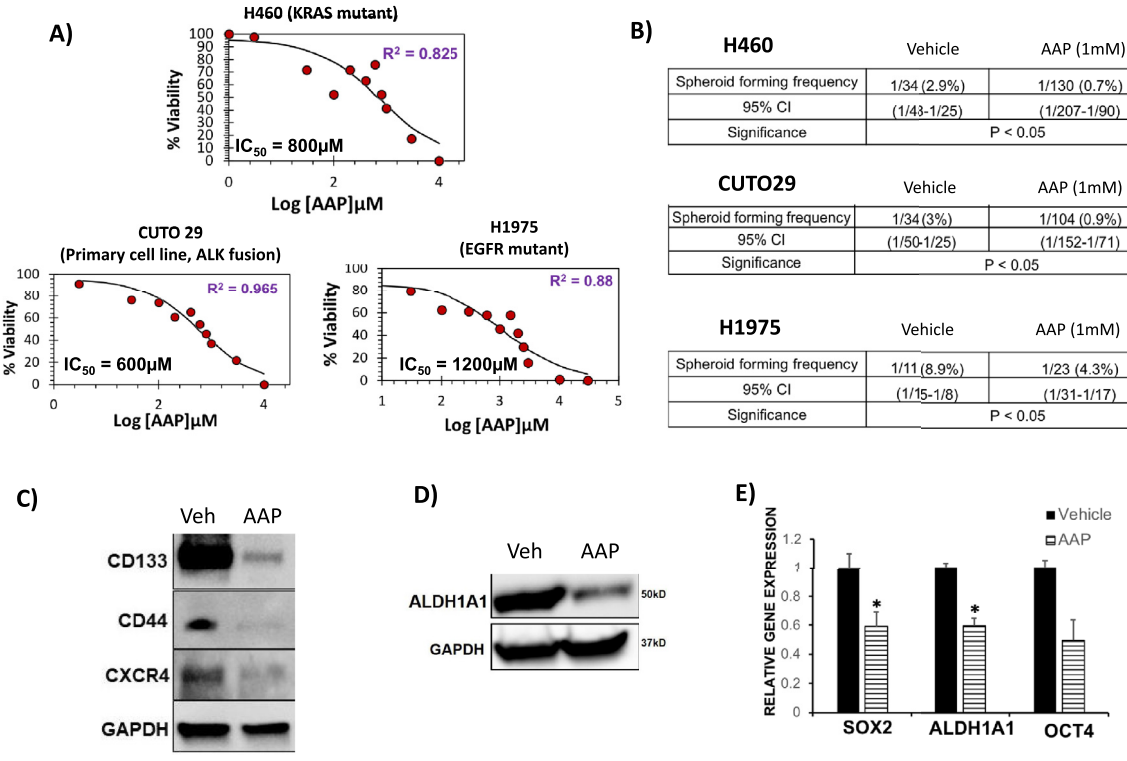


**Fig. 2.** Acetaminophen (AAP) inhibits CSC growth, self-renewal and CSC marker expression in vitro.
**(A)** Dose response curves of AAP for primary spheroid inhibition in selected NSCLC cell lines and primary human tumor-derived cells. Sigma plots software was used to determine $IC_{50}$ of spheroid formation. H460, CUTO29 and H1975 cells were plated in CSC media with increasing concentrations of AAP. Four days later, the number of spheroids per well 50-150 $\mu$M was counted. Results reported as percent of untreated vehicle. **(B)** In vitro limiting dilution assay (LDA) of H460, CUTO 29 and H1975 NSCLC cells. Cells were treated with vehicle or AAP for 24 h and then plated in fresh CSC media (no treatment) in limiting dilutions (0→128 cells /well). Four days after plating, wells were assessed for spheroid formation (yes/no). **(C to E)** H460 NSCLC cells were grown in CSC media as spheroids and treated for 24 h with DMSO (veh) or AAP (1 mM) prior to harvesting. **(C, D)** Immune-blot analyses for CSC markers, and **(E)** quantitative real-time PCR analyses for self-renewal factors in vehicle and AAP treated samples. (n = 3, 2 independent experiments). * $P < 0.05$.

and CUTO29 cells (EML4-ALK rearranged, patient-derived cell line); a 14-fold (A549 cells) and 13-fold (CUTO29 cells) increase in SFF in the CD133 high cells versus CD133 low cells was observed (Supplemental Figures 2, 3). These results suggest that CD133 functions as a CSC marker in NSCLC with diverse driver mutations.

We next performed an in vivo LDA to evaluate whether CD133 can be used as a marker of tumor initiating cells in NSCLC. H460 cells were flow-sorted to separate CD133 high and CD133 low cells. The cells were implanted in NCr nude mice in a limiting dilution, implanting 2K, 5K, 10K, 50K and 100K cells subcutaneously (4 mice per condition). Tumor size over 150 $mm^3$ was assessed on day 55 (yes/no). Using ELDA software, it was determined that CD133 high cells had a 5-fold increase in tumor initiating cell frequency compared to CD133 low cells (Fig. 1B). Additionally, tumors generated with CD133 high cells grew at a significantly increased rate relative to tumors generated with CD133 low cells (Fig. 1C).

*Acetaminophen has anticancer stem cell activity*

AAP and cisplatin both inhibited cell viability of H460 NSCLC in 2D monolayer culture. In monolayer, the $IC_{50}$ of H460 NSCLC cells was 4.6 mM for acetaminophen, and 0.8 $\mu$g/mL (2.7 µM) for cisplatin. In order to see if AAP had antiproliferative effects in other tumor types in addition to NSCLC, A2058 melanoma cells were also analyzed. In monolayer, the $IC_{50}$ for A2058 cells was 3.5 mM for acetaminophen and 0.5 $\mu$g/mL (1.7 µM) cisplatin (Supplemental Figure 4).

When grown in serum-free stem cell media, only AAP but not cisplatin treatment prevented 3D tumor spheroid formation in a dose-dependent manner (Supplemental Figure 5). Cultures treated with 3 mM AAP (which is less than the IC50 in both cell lines) led to >50% reduction in tumor spheroids, whereas 10 mM AAP led to complete elimination of spheroid formation in both H460 and A2058 cells. Cisplatin (0.5 or 2 $\mu$g/mL, which is well above the IC50 of both lines in monolayer) showed no effect on 3D tumor spheroids formation. These results suggest that AAP but not cisplatin has anti-CSC properties.

Analysis was performed in order to determine the $IC_{50}$ of AAP for inhibition of spheroid formation. NSCLC cells were plated into CSC medium along with increasing concentrations of AAP. The $IC_{50}$ value of H460 cells (*KRAS* mutant) was 800 $\mu$M, for CUTO29 (*EML4-ALK* fusion) was 600 $\mu$M and for H1975 (*EGFR* mutant) was 1200 $\mu$M (Fig. 2A). These results suggest that AAP inhibits spheroid growth in tumor cells with diverse oncogenic mutations. Of note, the $IC_{50}$ concentration for all the NSCLC cell lines tested are well below the maximum serum concentration of AAP that has been safely achieved (2.6 mM) in clinical trials, when given with NAC rescue [2].

The in vitro limiting dilution assay (LDA) is a widely used method of quantifying the stem cell frequency [17]. NSCLC cells with diverse driver mutations were grown in serum free CSC media and treated for 24 h with 1 mM AAP (near the $IC_{50}$ of spheroid formation of the tested cell lines). The cells were then plated for analysis by the LDA in treatment-free media. The AAP-treated cells had a 4-fold lower spheroid forming frequency (SFF) in H460 NSCLC cells, a 3-fold lower SFF in CUTO 29 cells, and a 2-fold lower SFF in H1975 cells (Fig. 2B) compared to respective vehicle-treated controls. As the SFF was determined in the absence of further treatment, the results

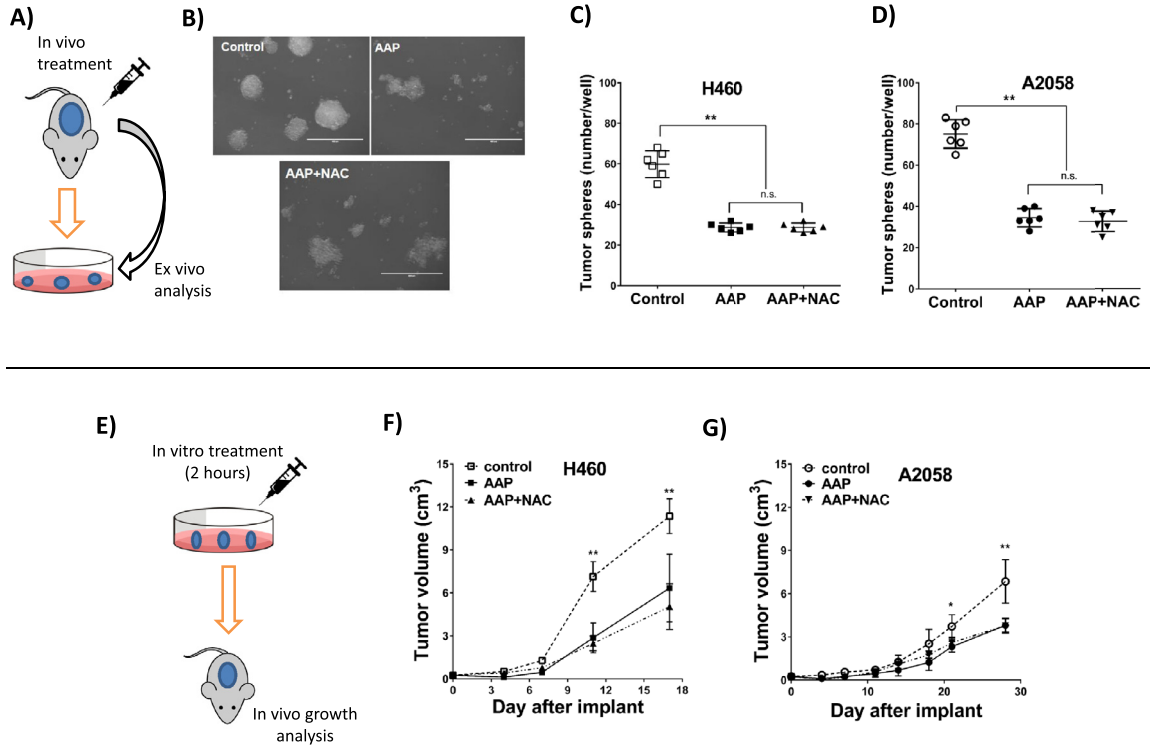


**Fig. 3.** Acetaminophen (AAP) reduces cancer stem cell growth and self-renewal in vivo. (**A–D**) In vivo treatment followed by ex vivo analysis. (**A**) Schema. Athymic rats were inoculated subcutaneously with 2.5 × $10^7$ A2058 melanoma cells **(B, D)** or H460 NSCLC cells **(C).** Rats (n = 3 per group) were untreated (control) or given AAP (600 mg/kg PO) with or without N-acetylcysteine (NAC, 1000 mg/kg IV) immediately after AAP at day 10 after inoculation. Tumors were harvested at day 14 after tumor implantation. Single tumor cell suspensions isolated from each subcutaneous tumor were cultured in tumor sphere stem cell media for 7 d. (**B**) Representative micrographs of A2058 cells, Scale bar = 400 $\mu$m. **(C, D)** Dot plots show number of tumor spheroids (50–150 $\mu$m) expressed as mean ± SD. **(E-G)** In vitro treatment followed by in vivo tumor growth analysis. (**E**) Schema. **(F)** H460 or **(G)** A2058 cells were untreated (control) or pretreated with AAP (10 mM) or AAP+NAC (1 mg/mL) for 2 h and then 2.5x$10^7$ cells were inoculated subcutaneously into the right and left flank of the athymic rat. Shown are subcutaneous tumor volumes over time; n = 6 for each condition, except N = 5 for AAP+NAC with A2058 cells. ** $P <$ 0.01, * $P < 0.05$.

suggest significant inhibition of CSC self-renewal by AAP. No significant change in spheroid size was observed with AAP treatment (Supplemental Figure 6A)

AAP treatment inhibited expression of CSC-related genes and markers in H460 NSCLC cells. Treatment with AAP resulted in suppressed expression of CSC markers CD133, CD44 and CXCR4 (Fig. 2C). AAP similarly decreased expression of ALDH1A1, another widely used CSC marker [26] (Fig. 2D). When evaluated using immunofluorescence, there was decreased intensity of CD44 staining in AAP-treated A2058 and H460 cells (Supplemental Figure 6B). At the RNA level, AAP decreased expression of the CSC-marker ALDH1A1 and the self-renewal regulating gene SOX2 (Fig. 2E). A trend suggested decreased expression of OCT4 as well.

Overall, AAP exhibits significant anti-CSC properties at clinically relevant concentrations in vitro.

*AAP inhibits CSC proliferation in vivo*

We next explored the ability of AAP to inhibit CSC growth/self-renewal in vivo in a rat subcutaneous xenograft model of A2058 and H460 cells. A single cell suspension was generated from tumors harvested from rats treated with a single dose of vehicle, AAP, or AAP+ NAC 4-d prior. When grown in stem cell media, the tumor cells from the AAP-treated or AAP+NAC-treated rats had significantly impaired ability to form 3D tumor spheroids relative to the tumors from the untreated rats (34.5 ± 4.4, 32.7 ± 4.9 vs 75.2 ± 6.9, respectively) suggesting inhibition of self-renewal. The spheroids obtained from the AAP and AAP + NAC treated rats were morphologically distorted and unhealthy appearing (Fig. 3A-D). These results support the anti-CSC properties of AAP *in vivo*, and suggest that NAC does not interfere with the anti-CSC effects of AAP.

As a functional test to evaluate the effects of AAP on CSCs, tumor cells were pretreated for 2 h with vehicle, AAP, or AAP + NAC in vitro and then injected into the flanks of nude rats (Fig. 3F, G). A 2-h incubation period approximates in vivo pharmacokinetics given that high-dose AAP has approximately a 2-4-h half-life [2]. Tumor cells that had been pretreated with AAP and/or NAC demonstrated significantly decreased and delayed growth compared to vehicle pretreated tumors (3.67 ± 1.68, 3.70 ± 1.04 vs 6.25 ± 1.08 g in H460; and 2.33 ± 0.61, 2.50 ± 0.62 vs 4.38 ± 1.28 g in A2058) (Supplementary Figure 7). These results suggest that tumor cells pretreated with AAP demonstrate impaired tumorigenic capacity, an effect not reversed by concurrent NAC treatment.

Overall, the above results suggest that in vivo or in vitro treatment with AAP inhibits CSC properties - self-renewal and tumor formation in vivo, respectively.

*AAP is a novel IL6/STAT3 inhibitor*

The presumptive mechanism of anticancer activity of high-dose AAP is analogous to its mechanism of hepatotoxicity, i.e., glutathione depletion and free radical mediated toxicity. In order to test this hypothesis, the relative effects of AAP on glutathione levels in the liver versus the tumor tissue harvested from NCr nude mice bearing H460 NSCLC xenograft following a

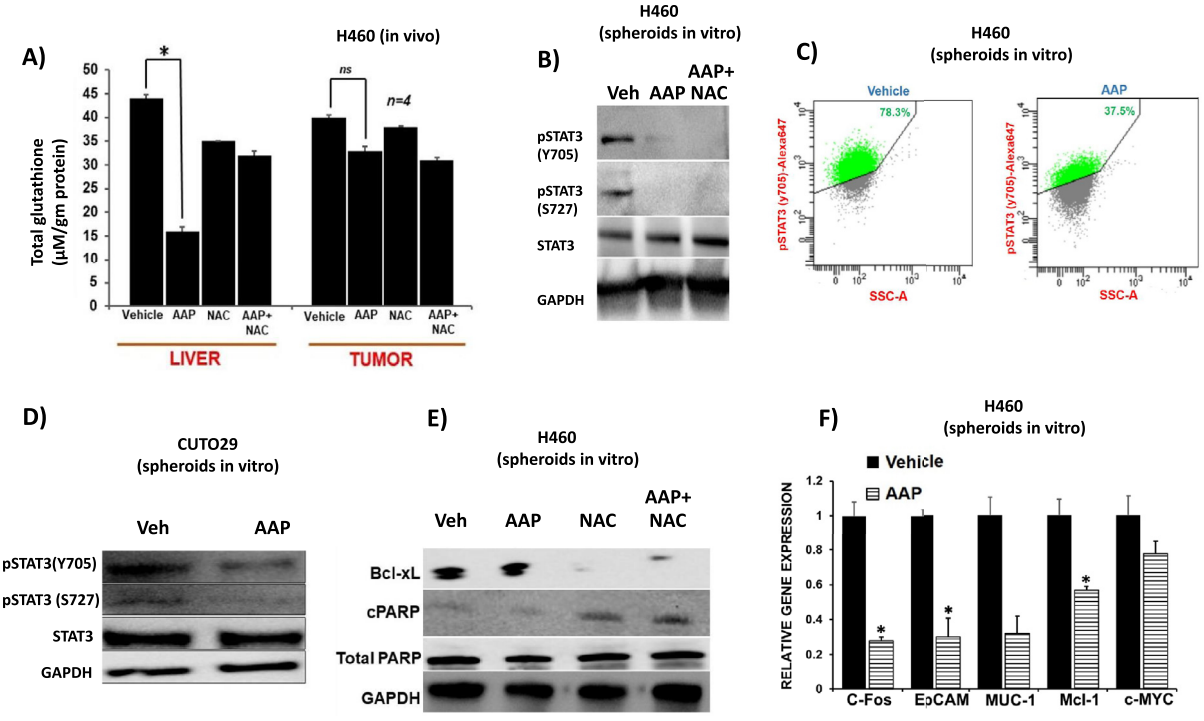


**Fig. 4.** Acetaminophen (AAP) inhibits STAT3 phosphorylation and nuclear function. (**A**) Mice were subcutaneously inoculated with $10^5$ H460 NSCLC cells. dWhen tumors reached 1200 $mm^3$, mice were treated with vehicle, AAP (500 mg/kg IP), and/or NAC (100 mg/kg IP). Mice were euthanized 4 h later and glutathione levels analyzed in tumors and livers, normalized to tissue weight**.** **(B)** H460 spheroids were treated for 24 h with AAP (1 mM), NAC (1 mg/mL) or vehicle and the cells were subjected to immune-blotting analysis or phospho-flow analysis **(C)**. **(D)** CUTO 29 NSCLC cells were grown in CSC medium and treated for 24 h with vehicle or AAP (1 mM) prior to immune-blotting analysis. (**E)** H460 NSCLC cells in cancer stem cell media were treated for 24 h with vehicle, AAP (1mM) and/or NAC (1 mg/mL). Cells were then collected and subjected to immune-blotting analysis. (**F)** qPCR analysis of mRNA from H460 spheroids treated with Vehicle or AAP (1mM) for 24 h (n = 3, 2 independent experiments). *** $P < 0.001$, * $P < 0.05$.

single dose of AAP (500 mg/kg) and NAC (100 mg/kg) were examined. AAP caused a significant decrease in glutathione levels in the liver but not in the tumor (Fig. 4A). Because NAC, the antidote for AAP toxicity, is a glutathione precursor, these results suggest that NAC may selectively rescue the liver but not the tumor from high-dose AAP treatment.

Because AAP does not exert anticancer activity via free radical-dependent mechanisms, we explored alternative potential mechanisms of anti-CSC activity using a semi-unbiased phosphokinase array. Phosphorylation of tyrosine 705 (Y705) and serine 727 (S727) of STAT3 was suppressed by AAP without affecting p-STAT5a/b status in both A2058 melanoma and H460 NSCLC cells (Supplemental Figure 8). WNK1, which has been shown to be involved in epithelial-mesenchymal transition in cancer cells [(27], was suppressed in both cell lines tested with AAP treatment. On the other hand, AAP increased pERK levels in both lines. However, increased pERK levels were not confirmed in immunoblotting experiments. SRC, a protein that can regulate STAT3 phosphorylation [28], did not have altered expression in AAP treated cells (Supplementary Figure 9). Due to the known role of STAT3 in the proliferation of CSCs, we focused our subsequent studies on AAP's effect on STAT3 phosphorylation and function.

To confirm the validity of the STAT3 inhibition seen in the phosphokinase array experiment, the phosphorylation status of STAT3 in AAP-treated cells was elucidated using immunoblotting experiments. Dose response experiments were performed to determine the concentrations of AAP necessary to inhibit STAT3 phosphorylation in melanoma A2058 cells grown in monolayer. It was found that AAP inhibits phosphorylation of STAT3 at Y705 starting at 1 mM concentrations with near complete inhibition at 10 mM concentrations (Supplementary Figure 10). AAP also inhibits phosphorylation of serine 727 (S727) on STAT3, achieving maximal inhibitory activity at 3 mM. AG490, a JAK inhibitor [29], inhibited STAT3 Y705 phosphorylation but not STAT3 S727 phosphorylation, a result consistent with the known distinct upstream regulatory mechanisms of Y705 and S727 [30].

We next evaluated the effect of AAP on NSCLC cells grown in CSC medium. 1 mM AAP inhibited STAT3 phosphorylation in H460 tumor spheroids (Fig. 4B), an effect not reversed by concurrent NAC administration. When evaluated using phospho-flow, AAP decreased the percent of STAT3 phosphorylated cells from 78% to 38% (Fig. 4C). AAP further inhibited STAT3 phosphorylation in patient-derived CUTO 29 NSCLC cells with an EML4-ALK rearrangement (Fig. 4D), suggesting that STAT3 is inhibited by AAP in cancer cells with diverse oncogenic mutations.

The kinetics of AAP-induced STAT3 inhibition was evaluated. AAP inhibited STAT3 phosphorylation starting at 4 h of treatment and this effect was sustained for 24 h (Supplementary Figure 11). Given that AAP has a half-life of about 2 to 4 h [31], we next aimed to determine if a brief pulse of AAP can result in sustained STAT3 inhibition. H460 NSCLC cells were treated with AAP in monolayer for 2 h (to approximate pharmacokinetic exposure in vivo) prior to changing medium and treating with NAC, sodium thiosulfate (STS) and/or interferon gamma (but no AAP). 24 h later, STAT3 inhibition was present in samples treated with AAP suggesting that brief pulses of high-dose AAP may achieve sustained STAT3 inhibition (Supplementary Figure 12).

We evaluated if free or radicals or glutathione metabolism may affect STAT3 phosphorylation. Buthionine sulfoximine (BSO), an inhibitor of glutathione synthesis, had no effect on STAT3 or STAT1 phosphorylation.

The antioxidants NAC and STS similarly did not affect the phosphorylation status of STAT3. These results suggest that AAP-induced changes in STAT3 phosphorylation may be free radical independent (Supplementary Figure 13).

The effects of AAP on STAT3 phosphorylation were evaluated ex vivo. A2058 tumors isolated 3 d after treatment with AAP (600 mg/kg PO) had decreased levels of phosphorylated STAT3 at both Y705 and S727 relative to vehicle-treated tumors (Supplementary Figure 14). A trend was observed suggesting decreased CD133 expression in the AAP treated tumors.

In our pretreatment tumor growth model (Fig. 3E), A2058 melanoma cells were treated for 2 h with AAP (+/- NAC) versus vehicle prior to implantation into the flanks of nude rats. Tumors were analyzed at time of sacrifice by immunofluorescence. Results demonstrated decreased expression of pSTAT3 and CD133 in the tumors that had been derived from cells treated with AAP (+/- NAC) relative to Vehicle control (Supplementary Figure 15).

We next aimed to evaluate if AAP inhibits STAT3 nuclear translocation and function. AAP inhibited IL-6-induced phosphorylation of STAT3 at Y705 in H460 and A2058 cells (Supplementary Figure 16). The staining pattern of Y705 phosphorylation STAT3 was nuclear, consistent with the known role that Y705 plays in regulating STAT3 nuclear function [32]. These results suggest that AAP inhibits pSTAT3 nuclear translocation.

The effects of AAP on expression of genes and proteins regulated by STAT3 were evaluated. AAP decreased protein levels of BCL-xL, an antiapoptotic protein that is downstream of STAT3 [33]. This effect was not reversed by NAC (Fig. 4E, Supplementary Figure 17). At the RNA level, AAP inhibited expression of multiple STAT3 regulated genes (Fig. 4F).

Taken together, these results suggest that AAP inhibits STAT3 phosphorylation, nuclear translocation, and transcriptional function in diverse cancer lines.

*AAP directly binds to STAT3 selectively over STAT1*

As AAP causes early and sustained inhibition of STAT3 in a free-radical independent fashion, we investigated if AAP directly binds STAT3 to inhibit its activation. Spectrofluorimetry is a method that reports the changes in the intrinsic fluorescence upon formation of protein–ligand complex [34] and can be used to calculate the affinity of the complex. STAT3 (22 nM) was titrated with AAP at 25°C while monitoring emission at 340 nm ($\lambda_{EX} = 280$ nm) using a PTI spectrofluorimeter (Fig. 5A). The change in fluorescence was clearly saturable suggesting formation of a STAT3– AAP complex. Nonlinear regression using a quadratic equation yielded an affinity of 3.8 $\mu$M**.** Interestingly, similar experiments with STAT1 showed essentially no change in fluorescence (Fig. 5B). The STAT3 inhibitor C 188-9 (also known as TTI-101) is currently being evaluated in clinical trials (NCT03195699). C 188-9 demonstrated direct binding to both STAT3 and STAT1, a result consistent with results of prior preclinical studies [35] (Fig. 5C, D). Ibuprofen was used as a negative control and demonstrated no binding to STAT3 or STAT1 at concentrations up to 0.1 mM (data not shown). Consistent with these results, AAP, but not C188-9, demonstrated specificity for inhibition of STAT3 phosphorylation relative to STAT1 in vitro (Fig. 5 E, F). AAP similarly did not inhibit STAT1 phosphorylation in cancer cells grown in monolayer culture (Supplemental Figure 18).

While both C188-9 and AAP inhibited spheroid formation of H460 cells in CSC medium as well as CD44 expression, only AAP (but not C188-9) suppressed expression of CD133 (Supplemental Figure 19).

In order to further validate the direct binding of AAP to STAT3, orthogonal approaches were used, namely microscale thermopheresis (MST) and a cellular thermal shift assay (Supplemental Figure 20). Using MST, AAP was shown to bind to STAT3 with a Kd of 0.6 +/- 0.4 $\mu$M. In the cellular thermal shift assay, increased expression of STAT3 in cells heated after treatment with AAP (+/- NAC) suggests ligand-induced stabilization of the protein at elevated temperatures, providing further evidence of direct binding of AAP to STAT3. The cellular shift assay results further suggest that NAC itself does not bind to STAT3, and, perhaps more importantly, does not interfere with STAT3 binding by AAP (Supplemental Figure 20).

*AAP inhibits CSC marker expression via a STAT3 dependent mechanism*

We next aimed to determine if the anti-CSC activity of AAP occurs via modulation of STAT3 activity. Transient knockdown (KD) of STAT3 in H460 NSCLC cells (Fig. 6) was achieved using shRNA. As expected, AAP (1 mM) inhibited spheroid formation by >50% in scrambled H460 cells compared to vehicle control. However, AAP had no effect on spheroid formation in the STAT3 knockdown cells compared to vehicle control, suggesting that AAP mediates its anti-CSC effects, in part, via STAT3 inhibition. At a molecular level, in further support of the spheroid formation findings, STAT3 KD cells showed inhibition of CSC marker CD133, phenocopying the effect of AAP. Also, AAP treatment only inhibited CD133 expression in scrambled but not STAT3 KD cells compared to vehicle control. Hence, STAT3 is a direct target of AAP and plays an important role in mediating its anti-CSC properties.

## Discussion

AAP is among the most commonly used drugs in the world as an antipyretic and analgesic. Drug repurposing for anticancer indications is a rapidly growing field which offers an efficient avenue for translating research into the clinic and offers distinct advantages over de novo drug discovery platforms. For instance, high-dose AAP has a pharmacologic and toxicological profile that is extremely well understood as a result of decades of research on the management of AAP overdose—culminating in the discovery of NAC as an antidote to AAP toxicity [5]. In fact, prompt administration of NAC in patients with markedly elevated blood AAP levels results in positive outcomes in the vast majority of patients; these results lay the foundation for the feasibility and safety of high-dose AAP with NAC rescue as a viable therapeutic approach [36,37].

The lack of advancement of high-dose AAP with NAC rescue to phase II clinical trials is unexpected given the promising phase I results—single agent high-dose AAP had a phase I response rate of 21% (3/14 assessable patients) [2]. Drugs with a 20% response rate or higher in phase I (less than 10% of drugs evaluated in phase I) have a 51% chance of meeting primary endpoints in subsequent phase II trials [38]. An incomplete mechanistic understanding of AAP's antitumor activity might have contributed to the lack of continued clinical development of high-dose AAP with NAC rescue. An additional barrier to advancement of earlier clinical trials was the impracticality of administering 20 g/m$^2$ of AAP orally (about 40 grams, or 80 extra strength acetaminophen tablets), leading to extreme nausea. However, an IV AAP formulation has since become FDA-approved (Ofirmev). In the current study, we aimed to provide a molecular foundation to prior clinical observations with a goal of reviving the probability of further preclinical and clinical study of high-dose AAP as an anticancer therapeutic.

For our in vitro studies, concentrations of AAP of 1-10 mM (~150–1500 $\mu$g/mL) are used. In the phase 1 dose escalation study of oral AAP, the maximal plasma AAP concentration was ~2.6 mM (400 $\mu$g/mL) in patients receiving 20 g/m$^2$ AAP without reaching a maximal tolerated dose [2]. In 2010, IV AAP was FDA approved as a parenteral analgesic. IV administration of AAP may lead to increased peak serum concentrations due to ease of administration (with reduced risk of associated nausea) and via bypassing first-pass metabolism in the liver. Further, our data suggest that NAC can be given concurrently with AAP, as opposed to the delayed time-points used in the initial clinical trials of high-dose AAP [2], without compromising the regimen's anti-CSC activity. Administering NAC concurrently with AAP is likely to improve the therapeutic index of high-dose AAP and reduce the risk of toxicity. Thus, with the advent of IV formulations of AAP and the potential for concurrent administration of IV AAP with IV NAC, concentrations of

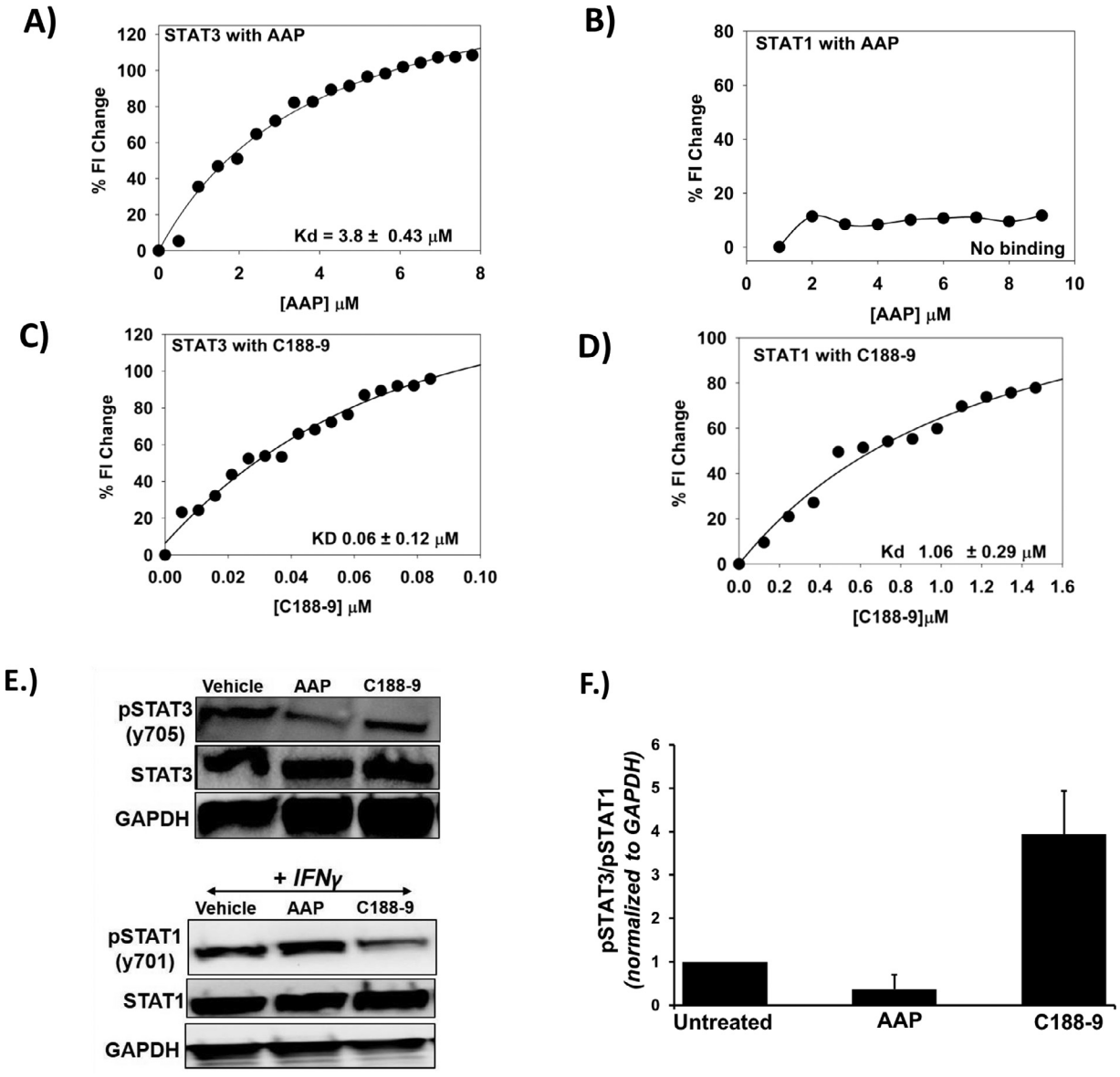


**Fig. 5.** Acetaminophen (AAP) binds to STAT3 with high specificity relative to STAT1. Spectrofluorimetry experiments were used to determine the binding affinity of AAP and C 188-9 to STAT3 **(A, C)** and STAT1 **(B, D). (E)** H460 NSCLC cells were grown in CSC medium and treated for 4 h with vehicle, AAP (1 mM) or C188-9 (10 $\mu$M). The cells were then collected and subjected to immune-blotting analysis. The blots were quantified using Image J software, and the pSTAT3/pSTAT1 ratio of 2 independent experiments was graphed, as shown in (**F**).

1 to 10 mM AAP may be achievable in carefully designed studies for the management of cancer patients.

Due to the known tumorigenic role of the STAT3 transcription factor, extensive efforts have been undertaken to develop selective inhibitors of STAT3 activation and phosphorylation. Unfortunately, there currently are no STAT3 inhibitors FDA approved for the management of cancer patients. One limitation faced by STAT3 inhibitors in clinical development is a relative lack of specificity for STAT3 over STAT1 [35]. Specificity for STAT3 over STAT1 is desirable because STAT3 appears to be pro-tumorigenic and STAT1 plays an important role in mediating the antitumor immune response [39]. Nevertheless, achieving specificity is challenging due to the high degree of homology between the proteins (53% identical and 72% similar) [40]. AAP, unlike other STAT3 inhibitors in clinical development [35,41], has a high degree of specificity for STAT3 relative to STAT1 (Fig. 5).

The possible mechanisms of STAT3 inhibition by AAP are direct or indirect. Mechanistically, S727 STAT3 is regulated by upstream signaling pathways including MEK-ERK [42], and JNK [43]. As demonstrated in Supplemental Figure 9, high-dose AAP has no effect of ERK phosphorylation. S727 on STAT3 can also be activated by nonreceptor tyrosine kinases, such as SRC [44]. SRC phosphorylation is not inhibited by AAP (Supplemental Figure 9). Y705 phosphorylation on STAT3 is most classically activated by gp130/JAK/STAT signaling. CD44 can mediate nuclear localization and activation of STAT3 via regulation of STAT3 acetylation [45] and Y705 phosphorylation [46,47]. Because AAP inhibits both Y705 and S727 phosphorylation, direct binding is the more likely mechanism given the distinct upstream regulatory pathways of the 2 residues [48] and their close physical proximity. Direct binding is further supported by the results of our spectrofluorimetry, MST, and cellular thermal shift binding studies (Fig. 5, Supplementary Figure 20).

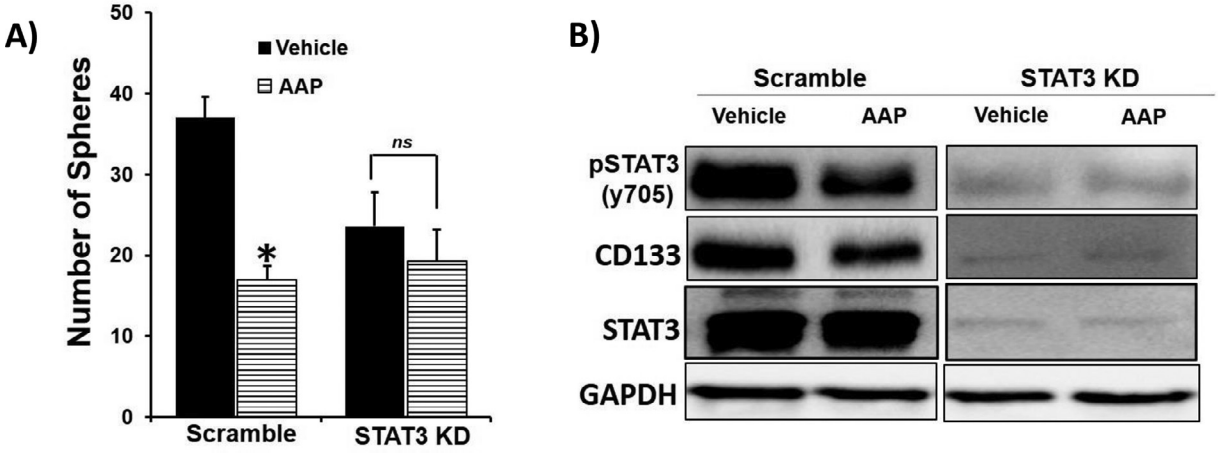


**Fig. 6.** AAP has anti-CSC activity via effects on STAT3. (**A**) H460 NSCLC cells were transiently transfected with STAT3 shRNA or scramble shRNA and then plated at 300 cells/well of 96-well plate. Cells were treated with vehicle or AAP (1 mM) and 3 d later the number of spheres per well 50–150 $\mu$M was quantified. (**B**) H460 cells transfected with shSTAT3 or scramble shRNA were treated with vehicle or AAP for 24 h and analyzed by immunoblotting. Note that a longer exposure is shown for the shSTAT3 knockdown cells due to suppressed signals in these cells.

Our research suggests several opportunities for future investigation. STAT3 is known to be involved in acquired resistance to targeted therapies in oncogene-driven cancers [49] and mediates cisplatin resistance in multiple malignancies [50,51]. Combination therapies of AAP with other targeted therapies (in targetable oncogene-driven malignancies) or cisplatin (in malignancies with or without a targetable mutation) may result in STAT3-mediated synergistic antitumor efficacy.

Currently, our lab is working on identifying the precise docking site of AAP on STAT3. Knowledge of the specific molecular interactions between AAP and STAT3 may allow for optimization of AAP-like daughter molecules rationally designed to provide potent and specific STAT3 inhibition.

In summary, we demonstrate that high-dose AAP acts as a novel inhibitor of STAT3 and CSCs, an effect not reversed by concurrent administration of NAC. These findings are of high clinical translational relevance and provide the mechanistic basis for a novel therapeutic approach for treating cancer patients with high-dose AAP administered concurrently with NAC for the selective rescue of the normal liver.

## Conflict of interest statement

OHSU and LLM have a financial interest in technology licensed to Fennec Pharmaceuticals, a company that may have a commercial interest in the results of this research and technology. This potential conflict of interest has been reviewed and managed by OHSU.

## Author contributions

Pavani Pignali: Investigation, validation.
Y. Jeffrey Wu: Investigation, validation.
Rio Boothelo: Supervision, methodology.
Chetna Sharon: Supervision, methodology.
Howard Li: Supervision.
Srinivas Sistla: Data curation.
Nehru Viji Sankaranarayanan: Data curation.
Umesh R. Desai: Data curation, methodology, supervision.
Anh T. Le: Resources
Robert C. Doebele: Resources
Leslie L. Muldoon: Funding acquisition, supervision.
Bhaumik B. Patel: Supervision, methodology, writing review and editing.
Alexander Neuwelt: Supervision, methodology, writing first draft.

## Funding

This study was supported by the Hunter Holmes McGuire VA Medical Center.

## Acknowledgment

The authors would also like to thank Ms. DreeAna Morris, Martha Joslyn and Samantha Holland for their excellent technical assistance. The studies presented in this work were carried out, in part, using the Biophysical Analysis and HT Screening and Imaging facility: (RRID): SCR_018832 of the Institute of Structural Biology Drug Discovery and Development, Virginia Commonwealth University. The CUTO29 cell line was derived using funding from the University of Colorado Lung SPORE grant (P50 CA058187). Services and products in support of the research project were generated by the VCU Massey Cancer Center Flow Cytometry Shared Resource, supported, in part, with funding from NIH-NCI Cancer Center Support Grant P30 CA016059.

## Supplementary materials

Supplementary material associated with this article can be found, in the online version, at doi:10.1016/j.neo.2021.02.001.

## References

[1] Neuwelt AJ, Wu YJ, Knap N, Losin M, Neuwelt EA, Pagel MA, Warmann S, Fuchs J, Czauderna P, Wozniak M. Using acetaminophen's toxicity mechanism to enhance cisplatin efficacy in hepatocarcinoma and hepatoblastoma cell lines. *Neoplasia* 2009;**11**:1003–11.

[2] Kobrinsky NL, Hartfield D, Horner H, Maksymiuk A, Minuk GY, White DF, Feldstein TJ. Treatment of advanced malignancies with high-dose acetaminophen and N-acetylcysteine rescue. *Cancer Invest* 1996;**14**:202–10.

[3] Wu YJ, Neuwelt AJ, Muldoon LL, Neuwelt EA. Acetaminophen enhances cisplatin- and paclitaxel-mediated cytotoxicity to SKOV3 human ovarian carcinoma. *Anticancer Res* 2013;**33**:2391–400.

[4] Kobrinsky NL, Sjolander DE, Goldenberg JA, Ortmeier TC. Successful treatment of doxorubicin and cisplatin resistant hepatoblastoma in a child with Beckwith-Wiedemann syndrome with high dose acetaminophen and N-acetylcysteine rescue. *Pediatr Blood Cancer* 2005;**45**:222–5.

[5] Heard KJ. Acetylcysteine for acetaminophen poisoning. *N Engl J Med* 2008;**359**:285–92.

[6] Bieche I, Narjoz C, Asselah T, Vacher S, Marcellin P, Lidereau R, Beaune P, de Waziers I. Reverse transcriptase-PCR quantification of mRNA levels from cytochrome (CYP)1, CYP2 and CYP3 families in 22 different human tissues. *Pharmacogenet Genomics* 2007;**17**:731–42.

[7] Visvader JE, Lindeman GJ. Cancer stem cells in solid tumours: accumulating evidence and unresolved questions. *Nat Rev Cancer* 2008;**8**:755–68.

[8] Clarke MF. Clinical and Therapeutic Implications of Cancer Stem Cells. *N Engl J Med* 2019;**380**:2237–45.

[9] Shiozawa Y, Nie B, Pienta KJ, Morgan TM, Taichman RS. Cancer stem cells and their role in metastasis. *Pharmacol Ther* 2013;**138**:285–93.

[10] Prieto-Vila M, Takahashi RU, Usuba W, Kohama I, Ochiya T. Drug Resistance Driven by Cancer Stem Cells and Their Niche. *Int J Mol Sci* 2017;**18**.

[11] Wei W, Tweardy DJ, Zhang M, Zhang X, Landua J, Petrovic I, Bu W, Roarty K, Hilsenbeck SG, Rosen JM, et al. STAT3 signaling is activated preferentially in tumor-initiating cells in claudin-low models of human breast cancer. *Stem Cells* 2014;**32**:2571–82.

[12] Marotta LL, Almendro V, Marusyk A, Shipitsin M, Schemme J, Walker SR, Bloushtain-Qimron N, Kim JJ, Choudhury SA, Maruyama R, et al. The JAK2/STAT3 signaling pathway is required for growth of CD44(+)CD24(-) stem cell-like breast cancer cells in human tumors. *J Clin Invest* 2011;**121**:2723–35.

[13] Galoczova M, Coates P, Vojtesek B. STAT3, stem cells, cancer stem cells and p63. *Cell Mol Biol Lett* 2018;**23**:12.

[14] Shao C, Sullivan JP, Girard L, Augustyn A, Yenerall P, Rodriguez-Canales J, Liu H, Behrens C, Shay JW, Wistuba II, et al. Essential role of aldehyde dehydrogenase 1A3 for the maintenance of non-small cell lung cancer stem cells is associated with the STAT3 pathway. *Clin Cancer Res* 2014;**20**:4154–66.

[15] Chan KS, Sano S, Kiguchi K, Anders J, Komazawa N, Takeda J, DiGiovanni J. Disruption of Stat3 reveals a critical role in both the initiation and the promotion stages of epithelial carcinogenesis. *J Clin Invest* 2004;**114**:720–8.

[16] Fisher DT, Appenheimer MM, Evans SS. The two faces of IL-6 in the tumor microenvironment. *Semin Immunol* 2014;**26**:38–47.

[17] Hu Y, Smyth GK. ELDA: extreme limiting dilution analysis for comparing depleted and enriched populations in stem cell and other assays. *J Immunol Methods* 2009;**347**:70–8.

[18] Bullock BL, Kimball AK, Poczobutt JM, Neuwelt AJ, Li HY, Johnson AM, Kwak JW, Kleczko EK, Kaspar RE, Wagner EK, et al. Tumor-intrinsic response to IFNgamma shapes the tumor microenvironment and anti-PD-1 response in NSCLC. *Life Sci Alliance* 2019;**2**.

[19] Jafari R, Almqvist H, Axelsson H, Ignatushchenko M, Lundback T, Nordlund P, Martinez Molina D. The cellular thermal shift assay for evaluating drug target interactions in cells. *Nat Protoc* 2014;**9**:2100–22.

[20] Swillens S. Interpretation of binding curves obtained with high receptor concentrations: practical aid for computer analysis. *Mol Pharmacol* 1995;**47**:1197–203.

[21] Wu YJ, Pagel MA, Muldoon LL, Fu R, Neuwelt EA. High alphav Integrin Level of Cancer Cells Is Associated with Development of Brain Metastasis in Athymic Rats. *Anticancer Res* 2017;**37**:4029–40.

[22] Kummarapurugu AB, Afosah DK, Sankaranarayanan NV, Navaz Gangji R, Zheng S, Kennedy T, Rubin BK, Voynow JA, Desai UR. Molecular principles for heparin oligosaccharide-based inhibition of neutrophil elastase in cystic fibrosis. *J Biol Chem* 2018;**293**:12480–90.

[23] Boothello RS, Al-Horani RA, Desai UR. Glycosaminoglycan-protein interaction studies using fluorescence spectroscopy. *Methods Mol Biol* 2015;**1229**:335–53.

[24] Zakaria N, Satar NA, Abu Halim NH, Ngalim SH, Yusoff NM, Lin J, Yahaya BH. Targeting Lung Cancer Stem Cells: Research and Clinical Impacts. *Front Oncol* 2017;**7**:80.

[25] Herheliuk T, Perepelytsina O, Ugnivenko A, Ostapchenko L, Sydorenko M. Investigation of multicellular tumor spheroids enriched for a cancer stem cell phenotype. *Stem Cell Investig* 2019;**6**:21.

[26] Tomita H, Tanaka K, Tanaka T, Hara A. Aldehyde dehydrogenase 1A1 in stem cells and cancer. *Oncotarget* 2016;**7**:11018–32.

[27] Hung JY, Yen MC, Jian SF, Wu CY, Chang WA, Liu KT, Hsu YL, Chong IW, Kuo PL. Secreted protein acidic and rich in cysteine (SPARC) induces cell migration and epithelial mesenchymal transition through WNK1/snail in non-small cell lung cancer. *Oncotarget* 2017;**8**:63691–702.

[28] Byers LA, Sen B, Saigal B, Diao L, Wang J, Nanjundan M, Cascone T, Mills GB, Heymach JV, Johnson FM. Reciprocal regulation of c-Src and STAT3 in non-small cell lung cancer. *Clin Cancer Res* 2009;**15**:6852–61.

[29] Xuan YT, Guo Y, Han H, Zhu Y, Bolli R. An essential role of the JAK-STAT pathway in ischemic preconditioning. *Proc Natl Acad Sci U S A* 2001;**98**:9050–5.

[30] Johnston PA, Grandis JR. STAT3 signaling: anticancer strategies and challenges. *Mol Interv* 2011;**11**:18–26.

[31] Rayburn W, Shukla U, Stetson P, Piehl E. Acetaminophen pharmacokinetics: comparison between pregnant and nonpregnant women. *Am J Obstet Gynecol* 1986;**155**:1353–6.

[32] Carpenter RL, Lo HW. STAT3 Target Genes Relevant to Human Cancers. *Cancers (Basel)* 2014;**6**:897–925.

[33] Al Zaid Siddiquee K, Turkson J. STAT3 as a target for inducing apoptosis in solid and hematological tumors. *Cell Res* 2008;**18**:254–67.

[34] Parikh HH, McElwain K, Balasubramanian V, Leung W, Wong D, Morris ME, Ramanathan M. A rapid spectrofluorimetric technique for determining drug-serum protein binding suitable for high-throughput screening. *Pharm Res* 2000;**17**:632–7.

[35] Jung KH, Yoo W, Stevenson HL, Deshpande D, Shen H, Gagea M, Yoo SY, Wang J, Eckols TK, Bharadwaj U, et al. Multifunctional Effects of a Small-Molecule STAT3 Inhibitor on NASH and Hepatocellular Carcinoma in Mice. *Clin Cancer Res* 2017;**23**:5537–46.

[36] Bateman DN, Dear JW, Thanacoody HK, Thomas SH, Eddleston M, Sandilands EA, Coyle J, Cooper JG, Rodriguez A, Butcher I, et al. Reduction of adverse effects from intravenous acetylcysteine treatment for paracetamol poisoning: a randomised controlled trial. *Lancet* 2014;**383**:697–704.

[37] Smilkstein MJ, Knapp GL, Kulig KW, Rumack BH. Efficacy of oral N-acetylcysteine in the treatment of acetaminophen overdose. Analysis of the national multicenter study (1976 to 1985). *N Engl J Med* 1988;**319**:1557–62.

[38] Bugano DDG, Hess K, Jardim DLF, Zer A, Meric-Bernstam F, Siu LL, Razak ARA, Hong DS. Use of Expansion Cohorts in Phase I Trials and Probability of Success in Phase II for 381 Anticancer Drugs. *Clin Cancer Res* 2017;**23**:4020–6.

[39] Avalle L, Pensa S, Regis G, Novelli F, Poli V. STAT1 and STAT3 in tumorigenesis: A matter of balance. *JAKSTAT* 2012;**1**:65–72.

[40] Trilling M, Le VT, Rashidi-Alavijeh J, Katschinski B, Scheller J, Rose-John S, Androsiac GE, Jonjic S, Poli V, Pfeffer K, et al. "Activated" STAT proteins: a paradoxical consequence of inhibited JAK-STAT signaling in cytomegalovirus-infected cells. *J Immunol* 2014;**192**:447–58.

[41] Assi HH, Paran C, VanderVeen N, Savakus J, Doherty R, Petruzzella E, Hoeschele JD, Appelman H, Raptis L, Mikkelsen T, et al. Preclinical characterization of signal transducer and activator of transcription 3 small molecule inhibitors for primary and metastatic brain cancer therapy. *J Pharmacol Exp Ther* 2014;**349**:458–69.

[42] Gough DJ, Koetz L, Levy DE. The MEK-ERK pathway is necessary for serine phosphorylation of mitochondrial STAT3 and Ras-mediated transformation. *PLoS One* 2013;**8**:e83395.

[43] Lim CP, Cao X. Serine phosphorylation and negative regulation of Stat3 by JNK. *J Biol Chem* 1999;**274**:31055–61.

[44] Johnson DE, O'Keefe RA, Grandis JR. Targeting the IL-6/JAK/STAT3 signalling axis in cancer. *Nat Rev Clin Oncol* 2018;**15**:234–48.

[45] Lee JL, Wang MJ, Chen JY. Acetylation and activation of STAT3 mediated by nuclear translocation of CD44. *J Cell Biol* 2009;**185**:949–57.

[46] Khurana SS, Riehl TE, Moore BD, Fassan M, Rugge M, Romero-Gallo J, Noto J, Peek RM Jr, Stenson WF, Mills JC. The hyaluronic acid receptor CD44 coordinates normal and metaplastic gastric epithelial progenitor cell proliferation. *J Biol Chem* 2013;**288**:16085–97.

[47] Chung SS, Aroh C, Vadgama JV. Constitutive activation of STAT3 signaling regulates hTERT and promotes stem cell-like traits in human breast cancer cells. *PLoS One* 2013;**8**:e83971.

[48] Huynh J, Chand A, Gough D, Ernst M. Therapeutically exploiting STAT3 activity in cancer - using tissue repair as a road map. *Nat Rev Cancer* 2019;**19**:82–96.

[49] Lee HJ, Zhuang G, Cao Y, Du P, Kim HJ, Settleman J. Drug resistance via feedback activation of Stat3 in oncogene-addicted cancer cells. *Cancer Cell* 2014;**26**:207–21.

[50] Gu F, Ma Y, Zhang Z, Zhao J, Kobayashi H, Zhang L, Fu L. Expression of Stat3 and Notch1 is associated with cisplatin resistance in head and neck squamous cell carcinoma. *Oncol Rep* 2010;**23**:671–6.

[51] Zhu X, Shen H, Yin X, Long L, Chen X, Feng F, Liu Y, Zhao P, Xu Y, Li M, et al. IL-6R/STAT3/miR-204 feedback loop contributes to cisplatin resistance of epithelial ovarian cancer cells. *Oncotarget* 2017;**8**:39154–66.